Neutron Diffraction Study of Mesoporous and Bulk Hematite, α-Fe_2O_3

A. H. Hill,*,† F. Jiao,‡,§ P. G. Bruce,§ A. Harrison,†,|| W. Kockelmann,⊥ and C. Ritter||

Centre for Science at Extreme Conditions, Erskine Williamson Building, The King's Buildings, The University of Edinburgh, Mayfield Road, Edinburgh, EH9 3JZ, United Kingdom, School of Chemistry, University of St. Andrews, North Haugh, St. Andrews, Fife, KY16 9ST, United Kingdom, Institut Laue-Langevin, 6 rue Jules Horowitz, 38042 Grenoble Cedex 9, France, and ISIS Facility, Rutherford Appleton Laboratory, Chilton, Didcot, OX11 0QX, United Kingdom

Received January 2, 2008. Revised Manuscript Received May 21, 2008

Variable temperature neutron diffraction was carried out on mesoporous α-Fe_2O_3 (hematite) with a mean pore diameter of 38.5 Å. Data were directly compared to measurements carried out on bulk hematite. Unlike bulk hematite, the mesoporous material does not undergo a spin−flop transition from a weak ferromagnet to a pure antiferromagnet (Morin transition, $T_M = 259.1(2)$). Instead, the material remains a weak ferromagnet down to 2 K with the magnetic moments staying perpendicular to the $R\bar{3}c$ [111] ([003] in the hexagonal cell) direction rather than realigning (to) almost parallel to this direction. The angle of the magnetic Fe^{3+} moments to the [111] direction in the antiferromagnetic state also accurately was obtained for bulk hematite. Using magnetic hysteresis measurements, the canting angle responsible for weak ferromagnetism within the *ab* planes (hexagonal setting) was deduced for the mesoporous material at 12 K and compared to the angle made in bulk hematite above T_M.

Introduction

There is currently a great deal of interest concerning the relationship between the dimensions of a material and its electronic, optical, or magnetic behavior. For example, the collective magnetic properties of materials may be modified strongly when they are prepared in the form of nanoparticles or rods, and this may have important consequences for their technological applications.[1–8] Recently, it was discovered that a wide range of materials may be prepared in mesostructured forms using a variety of templating techniques.[9–13] A particularly interesting development in the context of collective magnetism was the demonstration that transition metal oxides may be prepared in mesostructured forms while retaining a high degree of crystallinity.[14–18] In the case of hematite (α-Fe_2O_3), this was shown to have a profound effect on magnetic behavior in comparison to bulk samples.[17] In this study, we explored the nature of this effect through neutron diffraction studies of magnetic correlations in conventional samples, as well as a sample with a mesostructure imposed on it (mesoporous α-Fe_2O_3).

Hematite possesses a rhombohedral corundum structure (space group $R\bar{3}c$),[19] and upon cooling through the Néel temperature ($T_N = \sim 955$ K) adopts a spin structure containing two ferromagnetic sublattices (Fe and Fe') coupled antiferromagnetically to each other. The moments are aligned approximately perpendicular to the rhombohedral axis (in the basal plane of the hexagonal setting) with a small canting of the magnetic sublattices toward each other caused by a Dzyaloshinsky−Moriya (DM) interaction.[20,21] This gives the material a small, net moment. Upon cooling further, through

* Corresponding author. E-mail: a.h.hill@ed.ac.uk.
† The University of Edinburgh.
‡ Current address: Lawrence Berkeley National Laboratory, Berkeley, CA 94720.
§ University of St. Andrews.
|| Institut Laue-Langevin.
⊥ Rutherford Appleton Laboratory.

(1) Bødker, F.; Hansen, M. F.; Koch, C. B.; Lefmann, K.; Mørup, S. *Phys. Rev. B: Condens. Matter Mater. Phys.* **2000**, *61*, 6826.
(2) Klausen, S. N.; Lefmann, K.; Lindgård, P.-A.; Kuhn, L. T.; Bahl, C. R. H.; Frandsen, C.; Mørup, S.; Roessli, B.; Cavadini, N.; Niedermayer, C. *Phys. Rev. B: Condens. Matter Mater. Phys.* **2004**, *70*, 214411.
(3) Zhao, Y. M.; Dunnill, C. W.; Zhu, Y. Q.; Gregory, D. H.; Kockenberger, W.; Li, Y. H.; Hu, W. B.; Ahmad, I.; McCartney, D. G. *Chem. Mater.* **2007**, *19*, 916.
(4) Puntes, V. F.; Krishnan, K. M.; Alivisatos, A. P. *Science (Washington, DC, U.S.)* **2001**, *291*, 2115.
(5) Park, S. J.; Kim, S.; Lee, S.; Khim, Z. G.; Char, K.; Hyeon, T. *J. Am. Chem. Soc.* **2000**, *122*, 8581.
(6) Hyeon, T. *Chem. Commun. (Cambridge, U.K.)* **2003**, 927.
(7) Park, J.; Kang, E. A.; Bae, C. J.; Park, J. G.; Noh, H. J.; Kim, J. Y.; Park, J. H.; Park, J. H.; Hyeon, T. *J. Phys. Chem. B* **2004**, *108*, 13594.
(8) Mørup, S.; Madsen, D. E.; Frandsen, C.; Bahl, C. R. H.; Hansen, M. F. *J. Phys.: Condens. Matter* **2007**, *19*, 213202.
(9) Behrens, P. *Angew. Chem., Int. Ed. Engl.* **1996**, *35*, 515.
(10) Antonelli, D. M.; Ying, J. Y. *Angew. Chem., Int. Ed. Engl.* **1995**, *34*, 2014.
(11) Antonelli, D. M.; Nakahira, A.; Ying, J. Y. *Inorg. Chem.* **1996**, *35*, 3126.
(12) Tian, Z. R.; Tong, W.; Wang, J. Y.; Duan, N. G.; Krishnan, V. V.; Suib, S. L. *Science (Washington, DC, U.S.)* **1997**, *276*, 926.
(13) Yang, P. D.; Zhao, D. Y.; Margolese, D. I.; Chmelka, B. F.; Stucky, G. D. *Nature (London, U.K.)* **1998**, *396*, 152.
(14) Wang, Y. Q.; Yang, C. M.; Schmidt, W.; Spliethoff, B.; Bill, E.; Schüth, F. *Adv. Mater.* **2005**, *17*, 53.
(15) Zhu, K. K.; Yue, B.; Zhou, W. Z.; He, H. Y. *Chem. Commun. (Cambridge, U.K.)* **2003**, 98.
(16) Tian, B. Z.; Liu, X. Y.; Yang, H. F.; Xie, S. H.; Yu, C. Z.; Tu, B.; Zhao, D. Y. *Adv. Mater.* **2003**, *15*, 1370.
(17) Jiao, F.; Harrison, A.; Jumas, J. C.; Chadwick, A. V.; Kockelmann, W.; Bruce, P. G. *J. Am. Chem. Soc.* **2006**, *128*, 5468.
(18) Jiao, F.; Bruce, P. G. *Adv. Mater.* **2007**, *19*, 657.
(19) Izyumov, Y. A.; Ozerov, R. P. *Magnetic Neutron Diffraction*; Plenum Press: New York, 1970.
(20) Dzyaloshinsky, I. *J. Phys. Chem. Solids* **1958**, *4*, 241.
(21) Moriya, T. *Phys. Rev.* **1960**, *120*, 91.

10.1021/cm800009s CCC: $40.75
Published on Web 07/08/2008

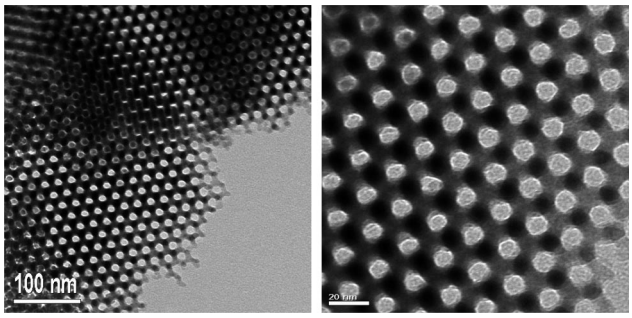

Figure 1. TEM images of mesoporous hematite, α-Fe_2O_3. The mesostructure is a 3-D negative replica of KIT-6.[17]

~260 K, the material undergoes a first order spin reorientation transition, called the Morin transition,[22] where the magnetic moments align themselves along the rhombohedral axis (the *c* axis of the hexagonal setting), and the net magnetic moment is lost. (The description of the magnetic structure of bulk hematite in ref 17 contains an error in the stated directions of the magnetic moments.) The temperature of the Morin transition is denoted as T_M. A slight inclination (tilt) of the moments away from the rhombohedral axis is present, leading to a residual component of the (111) peak in the magnetic diffraction patterns.[23] Analysis of the intensity of this peak enables the angle of tilt to be determined. Previous studies report this angle in the range of 5−15°.[23–25]

A large amount of work has been carried out concerning the relationship between particle size and magnetic ordering, with regard to the suppression of the Morin transition in hematite.[1,26–28] Susceptibility measurements were used recently to show that crystalline mesoporous α-Fe_2O_3 (surface area of 139 $m^2\ g^{-1}$, pore diameter of 38.5 Å) does not show a sharp decrease of the magnetic moment at T_M for the bulk material, or indeed at any temperature down to 2 K, while complementary neutron scattering data taken at 295 K indicate the same type of long-range magnetic order as found in bulk samples.[17] This suggests that the mesostructure leads to a suppression of the Morin transition. In this paper, we present neutron diffraction data taken with the same mesoporous hematite sample (Figure 1) from our previous paper[17] over a much wider range of temperatures. This provides the first thorough characterization of the crystallographic and magnetic structures of this new form of hematite down to 2 K, including the absence of a Morin transition. We also report the evolution of the crystallographic and magnetic structure of bulk hematite for comparison and reference, using data of the same or comparable quality, and allow refinement of the spin structure below T_M with a higher precision than previously was reported.

The synthesis and characterization of the mesoporous hematite sample previously was discussed,[17] so we shall only describe it briefly. An initial mesoporous silica template, KIT-6, was prepared as described by Ryoo and co-workers.[29] This has a 3-D pore structure with a cubic $Ia\bar{3}d$ asymmetric unit. Iron (III) nitrate was allowed to diffuse into the pore structure and was heated to decompose into iron (III) oxide. The silica template was subsequently removed by dissolving in NaOH, leaving a 3-D negative image Fe_2O_3 framework of the original mesoporous silica. TEM images (previously published) show a cubic structure of space group $Ia\bar{3}d$. Low-angle X-ray powder diffraction showed a peak corresponding to the (211) reflection, a_0 of 229 Å. Pore diameter and surface area were calculated from physisorption isotherms.

Experimental Procedures

Bulk hematite was obtained from Acros Organics, 99.999%, 100 mesh (diameter less than ~150 μm). Mesoporous hematite with a surface area of 139 $m^2\ g^{-1}$ and a pore diameter centered at 38.5 Å was prepared using a mesoporous silica template as previously described.[17] Diffraction measurements for bulk hematite were made from 10 to 300 K on a GEM diffractometer with a closed cycle refrigerator using six detector banks at the ISIS Facility. Data for the mesoporous sample were collected from 2 to 295 K on the time-of-flight spectrometer OSIRIS, also at ISIS, contained in a vanadium can and an Orange cryostat. Further neutron diffraction data were collected on diffractometer D1B at the Institut Laue-Langevin on bulk hematite to study in greater detail the evolution of the (111) peak with increasing temperature from 2 to 300 K.

Magnetic hysteresis and magnetization dependence with temperature measurements were performed using polycrystalline samples with a MPMS Quantum Design SQUID magnetometer. The samples were encapsulated in eicosane ($C_{20}H_{42}$, melting point 310 K) in gelatin capsules to prevent grain reorientation in strong magnetic fields.

Results

A $R\bar{3}c$ (hexagonal setting) crystallographic hematite model was fitted to the data sets as a nuclear model for the unit cell, with Fe and O atoms on the 12*c* and 18*e* crystallographic sites, respectively. A second phase consisting of 12 Fe atoms set at the positions generated by the symmetry operations of the $R\bar{3}c$ phase was added with *P*1 symmetry for refinement of the magnetic structure, following the two-phase fit without magnetic symmetry approach summarized by Cui et al.[30] Rietveld refinement[31] of the data was then carried out using the GSAS[32] suite of programs with the EXPGUI interface,[33] using typically 12 point shifted Chebyschev background polynomials for each diffraction pattern.

Bulk Hematite. Crystallographic and magnetic information obtained at the temperatures studied are shown in Table 1. Above T_M, the refinement was carried out with only the magnetic moment in the *x* direction allowed to refine, m_y was set to zero because the direction of the moments in the

(22) Morin, F. J. *Phys. Rev.* **1950**, *78*, 819.
(23) Morrish, A. H.; Johnston, G. B.; Curry, N. A. *Phys. Lett.* **1963**, *7*, 177.
(24) Nathans, R.; Pickart, S. J.; Alperin, H. A.; Brown, P. J. *Phys. Rev. A: At., Mol., Opt. Phys.* **1964**, *136*, 1641.
(25) Krén, E.; Molnàr, B.; Svàb, E.; Zsoldos, É. *Solid State Commun.* **1974**, *15*, 1707.
(26) Morrish, A. H. *Canted Antiferromagnetism: Hematite*; World Scientific: London, 1994.
(27) Zysler, R. D.; Fiorani, D.; Testa, A. M.; Suber, L.; Agostinelli, E.; Godinho, M. *Phys. Rev. B: Condens. Matter Mater. Phys.* **2003**, *68*, 212408.
(28) Muench, G. J.; Arajs, S.; Matijevic, E. *Phys. Status Solidi A* **1985**, *92*, 187.
(29) Kleitz, F.; Choi, S. H.; Ryoo, R. *Chem. Commun. (Cambridge, U.K.)* **2003**, 2136.
(30) Cui, J.; Huang, Q.; Toby, B. H. *Powder Diffraction* **2006**, *21*, 71.
(31) Rietveld, H. M. *J. Appl. Crystallogr.* **1969**, *2*, 65.

Table 1. Refined Crystallographic and Magnetic Data for Bulk α-Fe_2O_3[a]

T (K)	a (Å)	c (Å)	Fe^{3+} z coordinate	O^{2-} x coordinate	m_x (μ_B)	m_z (μ_B)	m (μ_B)	R_{wp}	R_p
300	5.035128(4)	13.75809(10)	0.355322(16)	0.30618(6)	4.118(6)	0	4.118(6)	0.0438	0.0419
250	5.034778(3)	13.74857(9)	0.355266(14)	0.30616(6)	1.607(10)	4.026(7)	4.165(7)	0.0411	0.0496
200	5.034516(4)	13.74145(10)	0.355169(15)	0.30615(6)	0.826(14)	4.101(7)	4.183(7)	0.0435	0.0516
150	5.034321(4)	13.73618(11)	0.355155(17)	0.30609(7)	0.785(16)	4.133(8)	4.207(8)	0.0493	0.0549
100	5.034172(4)	13.7321(11)	0.355082(17)	0.30605(7)	0.783(16)	4.164(8)	4.237(8)	0.0503	0.0487
50	5.034172(4)	13.73213(12)	0.355131(18)	0.30615(7)	0.762(18)	4.153(9)	4.223(9)	0.0554	0.0598
10	5.034171(4)	13.73210(11)	0.355080(17)	0.30602(7)	0.781(17)	4.149(9)	4.222(9)	0.0529	0.0520

[a] Data refined in the hexagonal setting of $R\bar{3}c$.

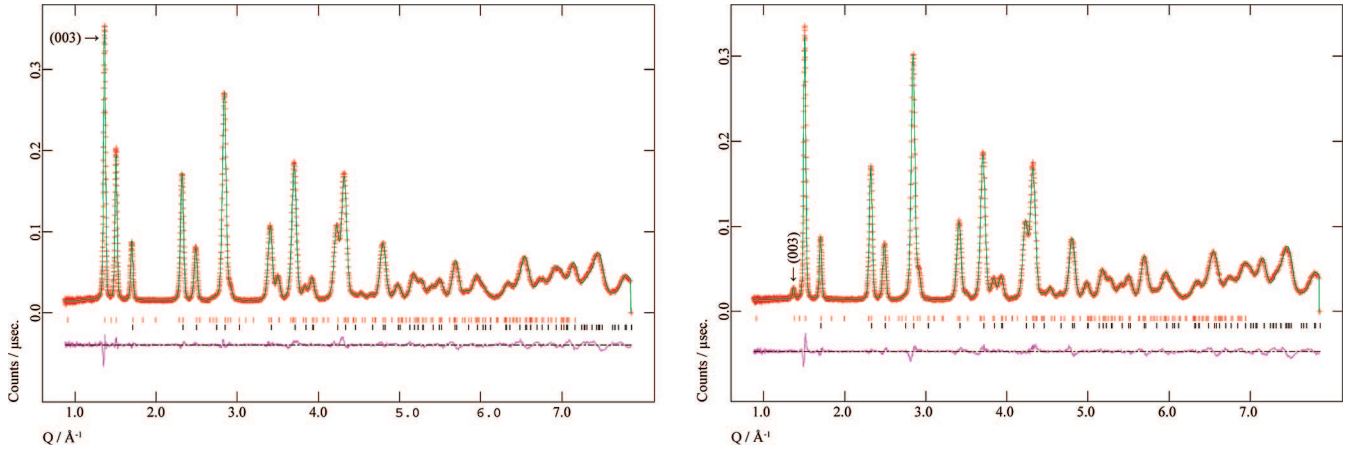

Figure 2. Observed and calculated neutron powder diffraction patterns from detector bank 3 of GEM for bulk α-Fe_2O_3 at 300 K (left) and 10 K (right). The difference pattern is shown below the patterns, with tick marks indicating the Bragg reflection positions from the nuclear, $R\bar{3}c$ (lower), and magnetic, $P1$ (upper), structures. The (003) Bragg reflection is marked.

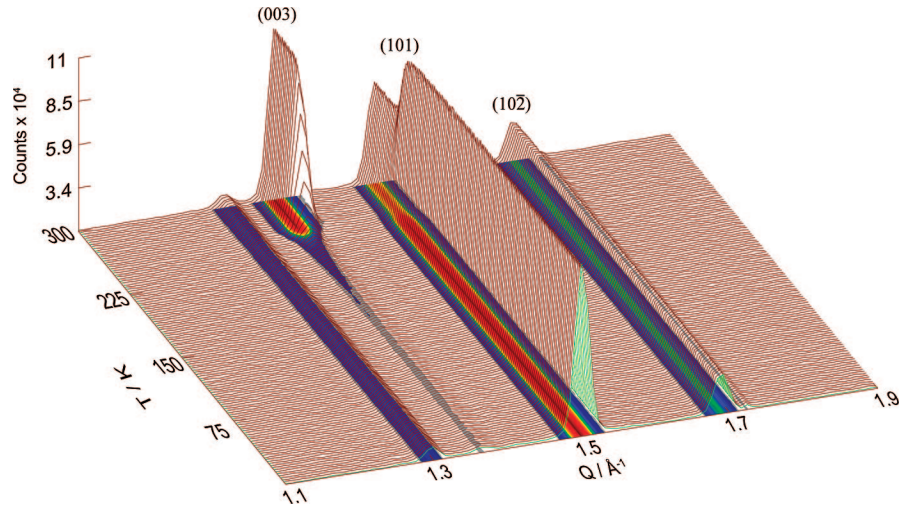

Figure 3. Neutron powder diffraction patterns from D1B of bulk α-Fe_2O_3 from 2 to 300 K. The (003) reflection can be seen at ~1.37 $Å^{-1}$. The peak at 1.3 $Å^{-1}$ is believed to be due to a low concentration of an impurity but does not affect the intensity of the (003) reflection.

hexagonal basal plane remain undetermined due to powder averaging, and m_z was set to zero as refinements with this included turned out to be unstable and diverging. Below T_M, magnetic moments in the x and z directions were allowed to refine (m_y set to zero, again due to powder averaging). Rietveld refinement patterns of neutron diffraction patterns collected on detector bank 3 of GEM above and below T_M, at 300 and 10 K, are shown in Figure 2. Data collected on D1B, tracing the change in Bragg peak intensities, are shown in Figure 3.

Mesoporous Hematite. Because of the limited Q space attainable on the OSIRIS instrument and high correlation between the thermal displacement parameters (U_{iso}) and the magnetic moment, the thermal displacement parameters in the mesoporous refinements were set at the values obtained from the bulk material on GEM. Unit cell parameters, atomic coordinates, and magnetic moments were then allowed to refine independently. These are presented in Table 2, with the omission of the 150 K data set due to a problem in the merging of the data sets, not allowing a full range of Q values in a continuous manner. Rietveld refinement patterns of neutron diffraction patterns collected at 295 and 2 K are

(32) Larson, A. C.; Von Dreele, R. B. *General Structure Analysis System (GSAS), Report No. LAUR 86-748*; Los Alamos National Laboratory: Los Alamos, NM, 2004.
(33) Toby, B. H. *J. Appl. Crystallogr.* **2001**, *34*, 210.

Table 2. Refined Crystallographic and Magnetic Data for Mesoporous α-Fe_2O_3[a]

T (K)	a (Å)	c (Å)	Fe^{3+} z coordinate	O^{2-} x coordinate	m_x (μ_B)	m_z (μ_B)	m (μ_B)	R_{wp}	R_p
295	5.03599(3)	13.7816(9)	0.35510(6)	0.3090(3)	4.05(2)	0	4.05(2)	0.0248	0.0188
250	5.036201(17)	13.7873(5)	0.35493(5)	0.3098(3)	3.98(2)	0	3.98(2)	0.0265	0.0190
100	5.035521(16)	13.7687(4)	0.35493(5)	0.3100(2)	4.192(18)	0	4.192(18)	0.0266	0.0224
50	5.035469(16)	13.7673(4)	0.35485(5)	0.3097(2)	4.208(18)	0	4.208(18)	0.0271	0.0231
2	5.035476(16)	13.7676(4)	0.35485(5)	0.3097(3)	4.224(18)	0	4.224(18)	0.0274	0.0235

[a] Data refined in hexagonal setting of $R\bar{3}c$. N.B. 295 K data sets were collected without the use of a cryostat. Because of different off-center sample displacements on the OSIRIS diffractometer for the two experimental settings (with and without cryostat), the lattice parameters for the mesoporous sample at 295 K are omitted in Figure 8.

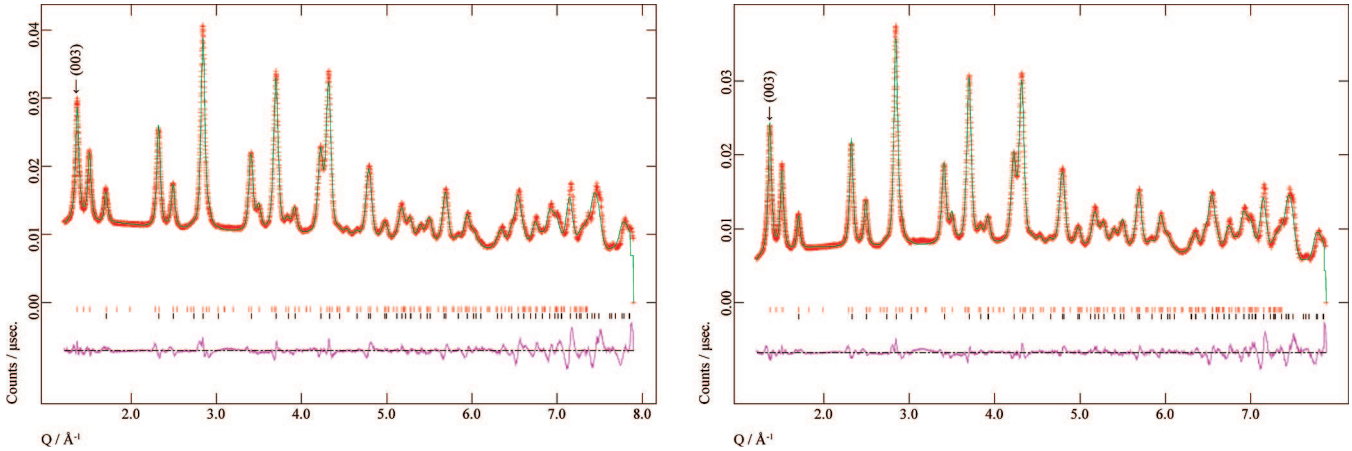

Figure 4. Observed and calculated neutron powder diffraction patterns from OSIRIS for mesoporous α-Fe_2O_3 at 295 K (left) and 2 K (right). The difference pattern is shown below the diffraction patterns, with tick marks indicating the Bragg reflection positions from the nuclear, $R\bar{3}c$ (lower), and magnetic, $P1$ (upper), structures. The (003) Bragg reflection is marked.

shown in Figure 4. For all data, the magnetic moments were refined as previously described for the bulk hematite sample above T_M.

Discussion

Bulk Hematite. From Figure 2, it can clearly be seen that as the temperature goes below T_M, the intensity of the (003) peak (in the rhombohedral setting, this corresponds to the (111) peak) changes dramatically to a much smaller finite value. The plot of integrated peak intensity (the FWHM of the (003) peaks in the D1B data was determined by fitting a Gaussian function to the peak with the ABFFIT software[34]) is shown in Figure 5, together with the refined moment on the Fe^{3+} ions from GEM data. The temperature at which the intensity of the (003) Bragg peak is halved from its maximum value is just above 254 K. This corresponds well to data taken in 0.01 T (cooled in zero field) with a MPMS Quantum Design SQUID magnetometer (Figure 5), which show T_M to be between 259.0 and 259.2 K (calculated to be the temperature at which the susceptibility is half that of the maximum value).

Above T_M, the magnetic structure was refined with no component along the c axis. As the intensity of the (003) reflection does not decrease to zero below T_M, it appears that there is a component of the magnetic moment on Fe^{3+} in the basal plane at a base temperature (Figure 6, produced with the VESTA program[35]). Rietveld refinement of a

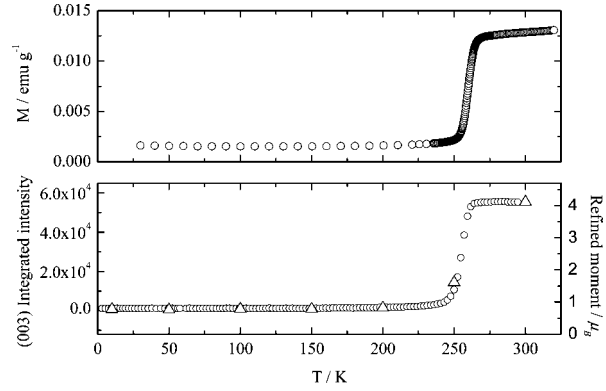

Figure 5. Magnetization (1 emu g^{-1} = 1 J T^{-1} kg^{-1}) of bulk α-Fe_2O_3 (upper) measured in 0.01 T (cooled in 0 T) and integrated peak intensity of the (003) Bragg peak of bulk α-Fe_2O_3 from D1B data (lower), showing the Morin transition. The calculated magnetic moment from refinement of GEM data in the *ab* plane also is shown (triangles). Error bars are of similar size as the data point symbols.

structure with such a component of that moment in the basal plane gave an estimate of the angle at which the moments tilt out away from the [111] direction. This angle was found to be 10.7(2)° at 10 K, which is in good agreement with, but more precise than, the previously published value of 15(10)°.[25] The values of the magnetic moments of the Fe^{3+} ions (m = 4.22(1) μ_B), calculated from the Rietveld refinements, are lower than that expected for the quantized z component of the spin-only moment of Fe^{3+}, 5.00 μ_B, but is of a similar value to previously refined values.[36] This is due to the α-Fe_2O_3 system being a charge transfer insulator

(34) Antoniadis, A.; Berruyer, J.; Filhol, A. *Acta Crystallogr., Sect. A: Found. Crystallogr.* **1990**, *46*, 692.
(35) Momma, K.; Izumi, F. *Commission Crystallogr. Comput., IUCr Newslett.* **2006**, *7*, 106.
(36) Baron, V.; Gutzmer, J.; Rundlöf, H.; Tellgren, R. *Solid State Sci.* **2005**, *7*, 753.

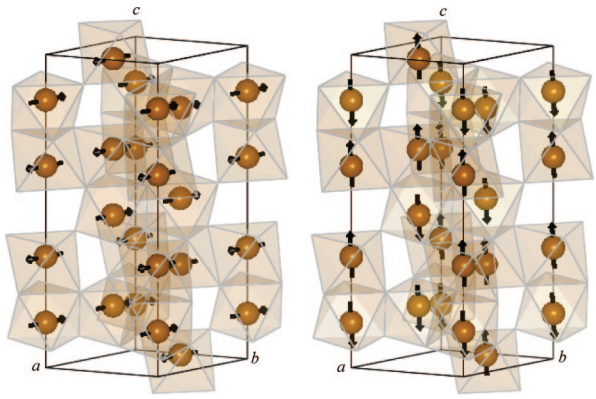

Figure 6. Arrangement of magnetic lattices in bulk hematite on either side of the Morin transition at 300 K (left) and 10 K (right).

rather than a Mott−Hubbard insulator[37,38] with a p−d band gap. Hence, there is a small amount of Fe−O σ-type bonding due to charge back transfer: $2p(O^{2-}) \rightarrow 3d(Fe^{3+})$. This therefore reduces the effective charge on the Fe^{3+} ions, producing a lower magnetic moment. This was observed with spherical neutron polarimetry in the case of isostructural eskolaite, Cr_2O_3.[39] No net magnetization is seen on the oxygen anions, due to an equal fraction of up and down spin gain from its up and down spin chromium cation neighbors.

Magnetic hysteresis loops of bulk hematite (Figure 7) carried out below and above T_M at 12 and 295 K show what is expected for the material. At 12 K, no hysteresis loop is observed, in line with what is expected for a simple antiferromagnet. At 295 K, hysteresis is observed, due to the weak ferromagnetic state of the material. Extrapolation of the high-field region of the **M**(**H**) curve (where saturation occurs) provides a spontaneous magnetization, $\mathbf{M}_r$, of 0.28 emu g^{-1}. This is of a similar magnitude to values previously reported.[26,40–42] In combination with the μ_B value obtained at the corresponding temperature by neutron diffraction, an *ab* plane canting angle λ of 0.06° can be calculated, corresponding to a canting component of 0.004 μ_B per Fe^{3+} ion, again agreeing with previous literature.[24] These results are summarized in Table 3.

Mesoporous Hematite. Rietveld refinement of the data for mesoporous hematite shows that no spin−flop transition occurs down to 2 K. This is made obvious by the (003) peak not diminishing in intensity (Figure 4). As with bulk hematite, the values of the calculated magnetic moments are lower than those expected for a free ion, again due to a loss of magnetic moment into the surrounding oxygen ligands; note too that iron at the surface of hematite has been shown to have a greatly reduced moment,[43] and the collective magnetic properties of hematite films have been observed to depart from those of bulk materials when their thickness is as much as 200 Å.[44]

When the temperature is reduced from 250 to 2 K, there is a considerable reduction in the background fit in the diffraction patterns, shown by a plot of background intensities (12 point shifted Chebyschev fit) over *Q* (Figure 8). A clear minimum can be seen in the lower temperature plots at ∼2.5 $Å^{-1}$; at lower *Q*, the background rises, due to slight overcompensation into the broadened Bragg peaks, which have the largest magnetic contribution.

Extraction of integrated peak intensities of the two purely magnetic (003) and (101) (the latter corresponding to the (100) peak in the rhombohedral setting) Bragg reflections using the CMPR program[45] shows an increase in area with cooling, corresponding to the reduction of the paramagnetic background (Figure 9). Despite problems with combining the full d-range of the 150 K data set for full Rietveld refinement, it was still possible to extract the peak areas. There are no components of the magnetic moments of Fe^{3+} ions in the [003] direction observable in any of the Rietveld refinements; all moments are 90° to this direction, in the basal plane. The material is, however, still a weak ferromagnet due to the DM interactions, causing a slight canting of the magnetic moments, distorting the alignment of the antiferromagnetic planes. Although this small ferromagnetic component of moment cannot be observed in our neutron diffraction patterns, it has been seen down to 2 K in magnetization measurements taken with the SQUID magnetometer.[17] As with bulk hematite, the canting angle can be calculated from the magnetic hysteresis curves (Figure 7) and with the calculated moments from the neutron diffraction data. At 12 K, the canting angle θ is 0.11°, corresponding to a spontaneous moment of 0.008 μ_B per Fe^{3+} ion (Table 3). What is particularly striking with the mesoporous material is that it is a much harder magnet at low temperatures. At 12 K, it has a coercive field ($\mathbf{H}_c$) of ∼0.36 T, as compared to ∼0.028 T at 295 K. This is similar to observations made in nanoparticulate hematite, where the higher coercive field was related to the existence of a higher anisotropy within the particles.[46] At room temperature, however, the bulk material is a harder magnet than the mesoporous material, $\mathbf{H}_c$ = ∼0.17 T.

Analysis of the refined lattice parameters of bulk and mesoporous hematite show that overall, the lattices of both bulk and mesoporous α-Fe_2O_3 contract upon cooling by approximately the same magnitude (0.02 and 0.2% along the *a* and *c* axes, respectively, in the bulk and 0.01 and 0.1% in the same respective directions in the mesoporous material). There is, however, a noticeable difference between the lattice parameters of the bulk and mesoporous samples. The lattice parameters are ∼0.03 and 0.3% greater in the mesoporous material along the *a* and *c* axes, respectively, than in bulk material throughout the temperature range studied (Figure 10). This gives a 0.2% increase in the *c*/*a* ratio for the mesoporous sample. Such lattice expansions previously were

(37) Catti, M.; Valerio, G.; Dovesi, R. *Phys. Rev. B: Condens. Matter Mater. Phys.* **1995**, *51*, 7441.
(38) Rollmann, G.; Rohrbach, A.; Entel, P.; Hafner, J. *Phys. Rev. B: Condens. Matter Mater. Phys.* **2004**, *69*, 165107.
(39) Brown, P. J.; Forsyth, J. B.; Lelievre-Berna, E.; Tasset, F. *J. Phys.: Condens. Matter* **2002**, *14*, 1957.
(40) Andersen, D. H. *Phys. Rev.* **1966**, *151*, 247.
(41) Goya, G. F.; Veith, M.; Rapalavicuite, R.; Shen, H.; Mathur, S. *Appl. Phys. A: Mater. Sci. Process.* **2005**, *80*, 1523.
(42) Flanders, P. J.; Remeika, J. P. *Philos. Mag.* **1965**, *11*, 1271.
(43) Wang, X. G.; Weiss, W.; Shaikhutdinov, S. K.; Ritter, M.; Petersen, M.; Wagner, F.; Schlögl, R.; Scheffler, M. *Phys. Rev. Lett.* **1998**, *81*, 1038.
(44) Kamzin, A. S.; Vcherashnii, D. B. *JETP Lett. (Engl. Transl.)* **2002**, *75*, 575.
(45) Toby, B. H. *J. Appl. Crystallogr.* **2005**, *38*, 1040.
(46) Zysler, R. D.; Winkler, E.; Vasquez Mansilla, M. V.; Fiorani, D. *Physica B* **2006**, *384*, 277.

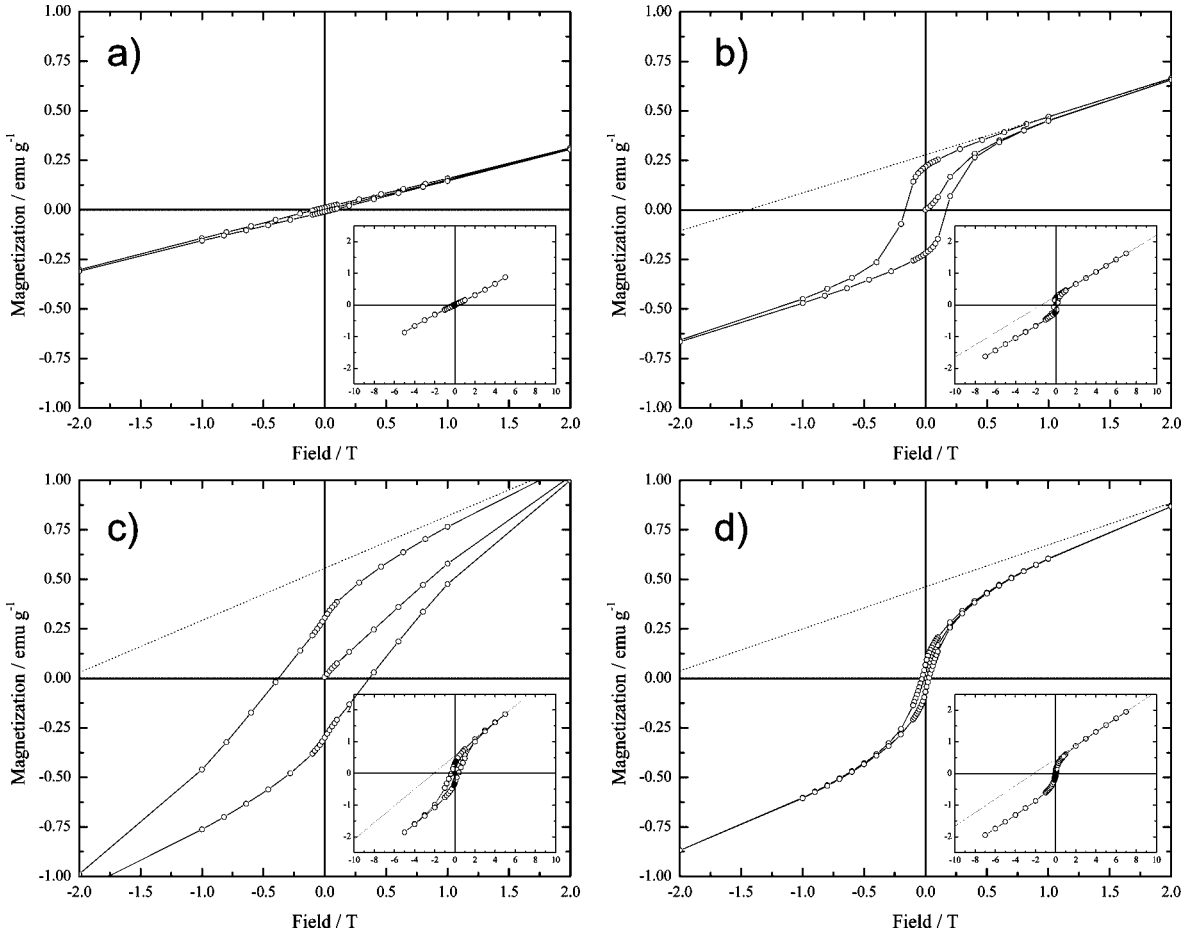

Figure 7. Magnetic hysteresis in bulk (a and b) and mesoporous (c and d) hematite at 12 K (a and c) and 295 K (b and d). All graphs are on the same scale for ease of comparison. Insets show full hysteresis loops. Dashed lines are linear fits to the high-field data to determine the remnant magnetizations in the weakly ferromagnetic states, $\mathbf{M}_r$.

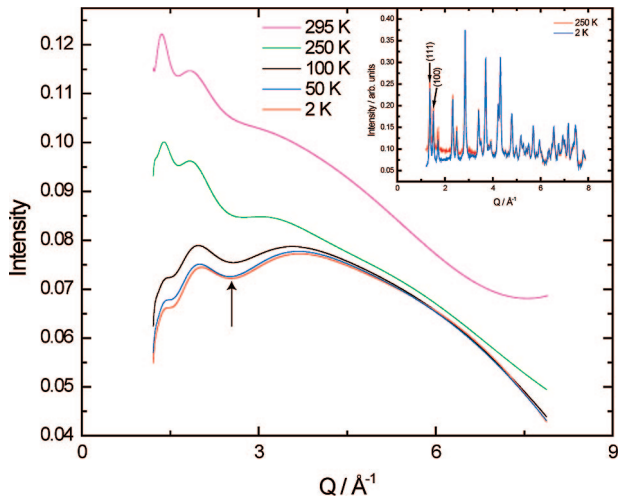

Figure 8. Plots of background functions for mesoporous α-Fe_2O_3 ranging from 295 K (top) to 2 K (bottom). The minimum marked with an arrow corresponds to a value of $Q = \sim 2.5$ Å^{-1}. Inset shows powder diffraction patterns of mesoporous α-Fe_2O_3 collected at 250 K (red upper pattern at low Q) and 2 K (blue lower pattern) with the pure magnetic (003) and (101) Bragg reflections marked. At low Q, a decrease of the paramagnetic background upon cooling is observed.

noted in microcrystalline hematite particles,[47–49] where a suppression of the Morin transition also was observed. Figure 11a shows as to how O−Fe−O angles in the FeO_6 octahedra change with temperature in both samples. The angles (Figure 12) are ∼78° (octahedral share a face along c between Fe and Fe') and 102° (no face sharing between Fe and Fe'). The dominant superexchange coupling is between spins on the two different antiferromagnetic sublattices (Fe and Fe'), which depend both on the Fe−O−Fe' bridging angle and Fe−O bond lengths. There are four different such Fe−O−Fe' bridging angles in the hematite cell;[37] two of ∼131°, one of ∼120°, and one of ∼86°; the corresponding Fe−O bond lengths are in the region of 3.7, 3.4, and 2.9 Å, respectively (Figure 12). The bridge closest to 90° is expected to have the weakest superexchange based on the Goodenough−Kanamori rules,[50] which are likely to override the fact that the corresponding bond lengths are the shortest.

When the unit cell dimensions a and c change, the angles and distances in the superexchange pathways will change. Expansion in a will lower the three angles that dominate the superexchange mechanism and increase the Fe−Fe' distances, both of which will reduce the superexchange. However, an expansion along c increases bridging angles (increasing superexchange), and bonds lengths (decreasing superexchange), with the effect that net antiferromagnetic

(47) Yamamoto, N. *J. Phys. Soc. Jpn.* **1968**, *24*, 23.
(48) Nininger, R. C.; Schroeer, D. *J. Phys. Chem. Solids* **1978**, *39*, 137.
(49) Schroeer, D.; Nininger, R. C. *Phys. Rev. Lett.* **1967**, *19*, 632.
(50) Goodenough, J. B. *Magnetism and the Chemical Bond*; Wiley Interscience: New York, 1963; p 15.

Table 3. Data from M(H) Curves and Calculated Canting Properties

sample	bulk Fe_2O_3 295 K	meso Fe_2O_3 295 K	meso Fe_2O_3 100 K	meso Fe_2O_3 12 K[a]
$\mathbf{H}_c$/T (estimated)	0.167	0.028	0.087	0.363
$\mathbf{M}_r$ (emu g^{-1})	0.278(3)	0.462(8)	0.54(2)	0.556(17)
θ (deg)	0.0554(8)	0.0934(20)	0.106(5)	0.108(2)
m_x/μ_B	4.118(6)	4.05(2)	4.192(18)	4.224(18)
m_y/μ_B	0.00380(6)	0.00661(17)	0.0078(4)	0.0079(2)

[a] Angle calculated using refined moment at 2 K.

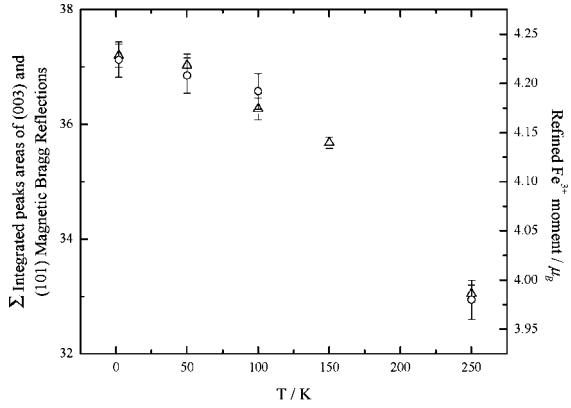

Figure 9. Sum of extracted integrated (003) and (101) Bragg peak intensities (triangles) and refined magnetic moment (circles) of mesoporous hematite, showing an increase in magnetic ordering with cooling.

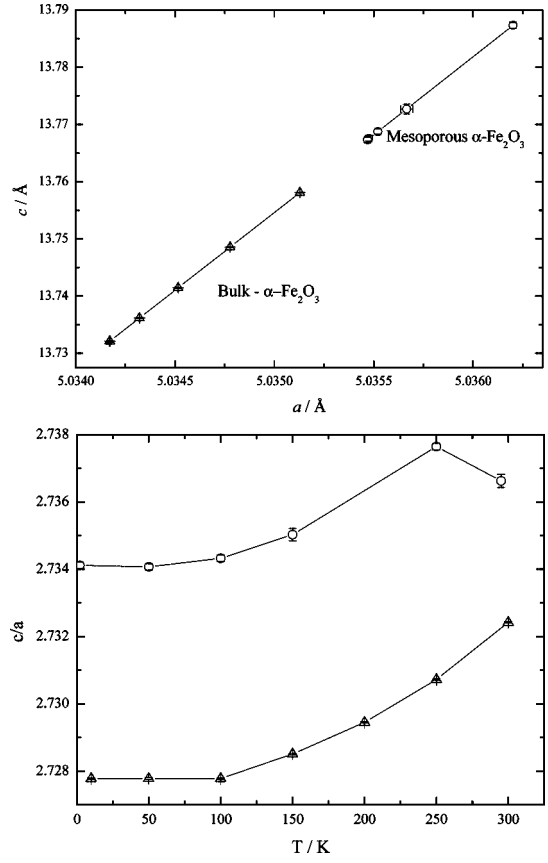

Figure 10. Plot of lattice parameters *c* and *a* (top) for bulk (triangles) and mesoporous (circles) hematite and variance of *c*/*a* ratio with temperature.

coupling is more sensitive to expansion along *a* than along *c*; if the ratio *c*/*a* is increased at a constant unit cell volume, antiferromagnetic coupling will become stronger. Figure 10 shows that *c*/*a* is larger for the mesoporous sample, while the volume of the unit cell is also larger at a given temperature, so it is unclear as to what the net effect will be.

The variation of geometry of these individual bridges with temperature and sample are presented graphically in Figure 11b−d. The strongest superexchange interaction is likely to propagate through the pathway with the largest bridging angle, whose properties are shown in Figure 11b: The angle in the bulk material is larger than in the mesoporous sample, while the length of this pathway is smaller. These two factors conspire to create a weaker superexchange interaction in the mesoporous material. However, when we take the other pathways into consideration, the picture is less clear. In general, bond lengths are greater at a particular temperature in the mesoporous sample, but there is no clear trend in the Fe−O−Fe' bridging angle, so it is difficult to say as to what the overall trend will be in the strength of the superexchange interaction with regard to the nature of the sample.

The diffraction patterns show clear Scherrer broadening of both magnetic and structural Bragg peaks of the mesoporous sample. This could be due to disruption of the repetition of the crystallographic and magnetic cell over long ranges by the mesostructure. Using TOF profile 2 in GSAS[32] (an incorporation of the Ikeda−Carpenter function[51] with a pseudo-Voigt linear combination of a Lorentzian and Gaussian function), the γ_2 variables of the Lorentzian part of the peak profile were allowed to refine independently between nuclear and magnetic phases. The nuclear and magnetic correlation lengths in the material were calculated using the Scherrer equation. Over the temperature range studied, the average values for the nuclear and magnetic correlation lengths were calculated to be 152.8(6) and 137.6(6) Å, respectively, in the mesoporous material. These are much shorter than those found in a sample of bulk α-Fe_2O_3 studied with the same experimental settings (300 and 150 K) with values of 529(4) and 594(5) Å for the nuclear and magnetic phases.

The spin orientation in bulk crystalline hematite is determined by a number of interactions in the material. The spin Hamiltonian can be expressed as follows:[52]

$$\mathcal{H} = \sum_{\langle ij \rangle} \{J_{ij}(\mathbf{S}_i \cdot \mathbf{S}_j) + \mathbf{D}[\mathbf{S}_i \times \mathbf{S}_j] + \mathbf{S}_i \cdot K_{ij} \cdot \mathbf{S}_j\} + \sum_i \{D\mathbf{S}_{iz}^2 + \mu_B \mathbf{S}_i \cdot g_i \cdot \mathbf{H}\} \quad (1)$$

The first term includes the Heisenberg exchange interaction, the Dzyaloshinsky−Moriya interaction, and the magnetic dipolar interactions. The second term concerns the single ion anisotropy and the Zeeman energies.

(51) Ikeda, S.; Carpenter, J. M. *Nucl. Instrum. Methods Phys. Res., Sect. A* **1985**, *239*, 536.

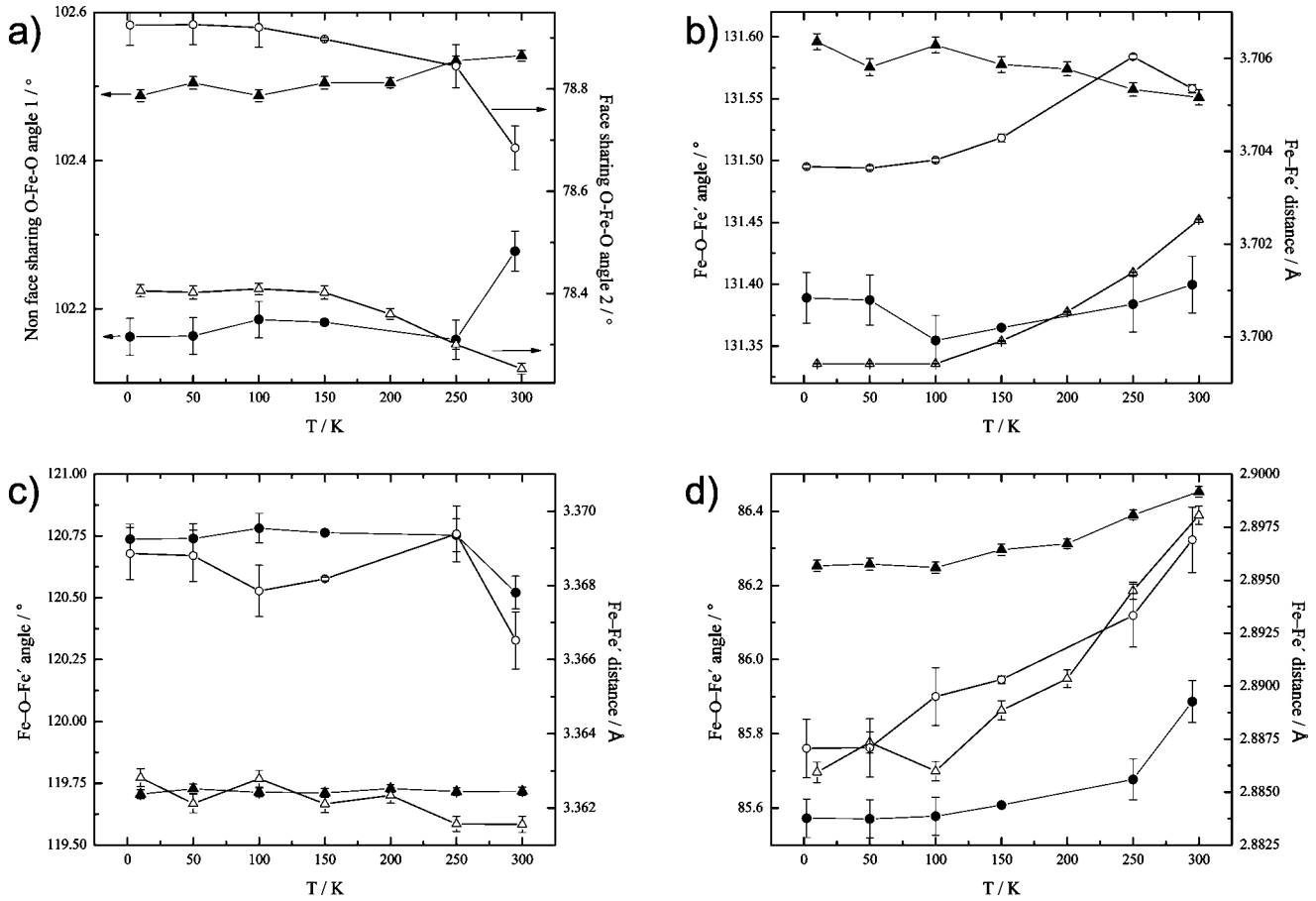

Figure 11. Structural characteristics of FeO_6 coordination polyhedra and Fe−O−Fe' exchange pathways for mesoporous (circles) and bulk (triangles) hematite. (a) O−Fe−O angles for face sharing (solid symbols) and nonface sharing (open symbols) parts of FeO_6 octahedra (see Figure 12). (b−d) Calculated Fe−O−Fe' angles (solid symbols) and Fe−Fe' distances (open symbols). Data points are connected purely to guide the eye.

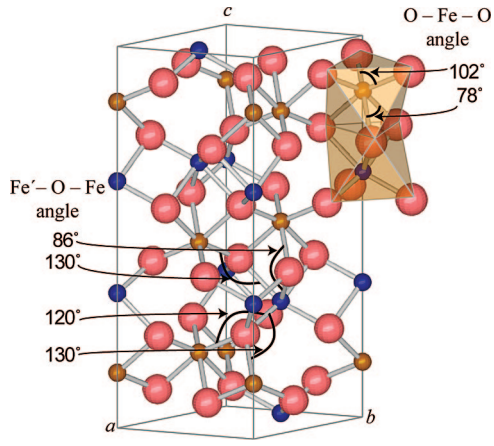

Figure 12. Hexagonal unit cell of hematite showing the Fe−O−Fe' angles for the different dominant superexchange pathways, as well as the O−Fe−O angles within each FeO_6 octahedra. The large spheres represent O^{2-}, and the small spheres represent the two different spin sublattices of Fe^{3+}: Fe (dark blue) and Fe' (light brown) (after Catti et al.[37]).

The spin reorientation at T_M arises from a change of sign of the total magnetic anisotropy E_{mag}.[26,53–55] This term is made up of several individual contributions; the magnetocrystalline anisotropy E_{mca} (involves noncubic components of the ligand field in conjunction with spin−orbit coupling), the shape anisotropy E_s (long-range dipolar anisotropy), and the surface anisotropy $E_{surface}$ (lower crystal symmetry and reduced coordination numbers)

$$E_{mag} = E_{mca} + E_s + E_{surface} \quad (2)$$

In bulk hematite, the two dominant terms are the magnetocrystalline anisotropy and the shape anisotropy. These two terms are very similar in magnitude (2% difference) but have opposite signs. At low temperatures in bulk hematite, the positive E_{mca} term dominates over the E_s term, causing the magnetic moments to be aligned parallel to the hexagonal axis. As T is raised, the negative E_s term has a greater influence, until it forces the spins to reorientate into the *ab* plane, causing the Morin transition. In the case of the mesoporous material, it can be deduced that the sign of the E_{total} term stays negative down to 2 K, similar to what is observed in hematite nanoparticles.[2] For this to happen, either the magnitude of the E_{mca} term must be reduced (less positive), the magnitude of the E_s term must be increased (more negative), or the total $E_{surface}$ must be decreased.

It is known that the shape anisotropy scales with M_s^2.[56,57] As the magnetic moments from the powder diffraction data

(52) Moriya, T., Weak ferromagnetism. In *Magnetism*; Rado, G. T., Suhl, H., Eds.; Academic Press: San Diego, 1963; Vol. 1, p 85.
(53) Artman, J. O.; Murphy, J. C.; Foner, S. *Phys. Rev.* **1965**, *138*, 912.
(54) Harrison, R. J.; McEnroe, S. A.; Robinson, P.; Carter-Stiglitz, B.; Palin, E. J.; Kasama, T. *Phys. Rev. B: Condens. Matter Mater. Phys.* **2007**, *76*, 174436.
(55) Wu, R., Theory of magnetocrystalline anisotropy and magnetoelasticity. In *Handbook of Magnetism and Advanced Magnetic Materials*; Kronmüller, H., Parkin, S., Eds.; John Wiley and Sons: New York, 2007; Vol. 1, p 423.
(56) Yoshida, K. *Prog. Theor. Phys.* **1951**, *6*, 691.

are comparable between bulk and mesoporous samples, it is unlikely that there is a vast difference between the E_s values. E_{mca} depends largely on the mean distortion of FeO_6 octahedra from their ideal form: The data presented in Figure 11a suggest that over most of the temperature range studied, the mesoporous material contains FeO_6 units closer to undistorted octahedra, but precisely as to how significant this effect will be on the stabilizing one spin structure over another would require precise calculations of E_{mca}. What is appreciable is the increase in surface area of the mesoporous sample. The effect of surface anisotropy was first postulated by Néel.[58] It has been shown that in thin metal films, the surface anisotropy can have a significant effect for thicknesses up to 600 Å.[52] Theoretical studies have shown how important the surface anisotropy is in nanoparticles and how this can vary with respect to the crystal plane at the surface.[59–61] Experimental observations of increased coercive fields (indicative of an increased surface anisotropy) also were reported in hematite nanoparticles.[46,62] In the case of nanoparticulate samples of diameter d, it has been shown that T_M scales linearly with $1/d$, implying that surface effects are the dominant influence.[27] Particles in the 80−200 Å diameter range have been shown to have no Morin transition even down to 4 K.[1,63–68]

The precise nature of such a surface effect has not been examined in detail but is likely to arise from variations in anisotropy and exchange fields that occur where the coordination of iron atoms deviates from that found in bulk material:[46] an effect that is likely to be much greater for the mesoporous materials in comparison to bulk compounds. To explore this further requires more detailed knowledge of the nature of the surface itself (i.e., the specific crystal planes found at the mesopore surfaces, their composition, and the extent of disorder), which is beyond the scope of this work.

Neutron scattering studies of collective magnetic excitations in hematite particles of 160 Å in diameter indicate that in contrast to bulk material, the sign of the magnetic anisotropy does not change from 300 K down to at least 50 K.[2] Studies of the magnetic excitations in mesoporous material by inelastic neutron scattering to obtain the magnetic anisotropy value would be desirable to unravel the various competing interactions and their variations with temperature.

Conclusion

From the variable temperature neutron diffraction of mesoporous α-Fe_2O_3, we have shown that this material does not undergo a first order spin reorientation transition down to 2 K. This is clearly evident from the (003) magnetic Bragg peak intensity not decreasing at low temperatures. If the Morin transition were to exist, it would be expected that the (003) Bragg peak would drop drastically, as seen in the bulk α-Fe_2O_3 reference sample at 259.1(2) K. Rietveld refinement of data taken from the bulk material below this temperature provides the most precise estimate to date of the canting of moments on Fe^{3+} ions from the hexagonal c axis, with a value of 10.7(2)° at 10 K. In the case of the mesoporous α-Fe_2O_3 sample, the spin structure at 2 K does not deviate from the one found above the Morin transition in the bulk material. It also was observed that the paramagnetic scattering from the mesoporous sample increased significantly with increasing temperature, despite the sample still being below the Néel ordering temperature (∼955 K in bulk α-Fe_2O_3,). No such increase in paramagnetic scattering was seen in the bulk material over a comparable temperature range. This suggests that there is rising surface disorder of the magnetic spins in the mesostructured material as the temperature is raised. Moreover, this suggests that the surface plays a key role in the magnetic properties of such mesoporous magnets. More detailed insights into the effect of temperature and mesostructure on the magnetic behavior of mesoporous hematite may be revealed by inelastic neutron scattering measurements of the magnetic excitations, in turn providing a measure of the changing contributions of competing terms in the Hamiltonian.

Acknowledgment. A.H.H. thanks Drs. A. J. Williams and J. A. Rodgers for their guidance with Rietveld refinements and Prof. J. P. Attfield and Drs. I. D. H. Oswald and S. A. J. Kimber for their useful input and suggestions. We also thank the referees for their very helpful suggestions.

CM800009S

(57) Tachiki, M.; Nagamiya, T. *J. Phys. Soc. Jpn.* **1958**, *13*, 452.
(58) Néel, L. *J. Phys. Radium* **1954**, *15*, 225.
(59) Zhang, K.; Fredkin, D. R. *J. Appl. Phys.* **1996**, *79*, 5762.
(60) Huang, Z.; Chen, Z.; Li, S.; Feng, Q.; Zhang, F.; Du, Y. *Eur. Phys. J. B* **2006**, *51*, 65.
(61) Restrepo, J.; Labaye, Y.; Greneche, J. M. *Physica B* **2006**, *384*, 221.
(62) Zysler, R. D.; Vasquez Mansilla, M.; Fiorani, D. *Eur. Phys. J. B* **2004**, *41*, 171.
(63) Kündig, W.; Bömmel, H.; Constabaris, G.; Lindquist, R. H. *Phys. Rev.* **1966**, *142*, 327.
(64) Amin, N.; Arajs, S. *Phys. Rev. B: Condens. Matter Mater. Phys.* **1987**, *35*, 4810.
(65) de Boer, C. B.; Mullender, T. A. T.; Dekkers, M. J. *Geophys. J. Int.* **2001**, *146*, 201.
(66) Gee, S. H.; Hong, Y. K.; Sur, J. C.; Erickson, D. W.; Park, M. H.; Jeffers, F. *IEEE Trans. Magn.* **2004**, *40*, 2691.
(67) Dang, M. Z.; Rancourt, D. G.; Dutrizac, J. E.; Lamarche, G.; Provencher, R. *Hyperfine Interact.* **1998**, *117*, 271.
(68) Wu, C. Z.; Yin, P.; Zhu, X.; OuYang, C. Z.; Xie, Y. *J. Phys. Chem. B* **2006**, *110*, 17806.